Iterative reconstruction of transmission sinograms with low signal to noise ratio.

Johan Nuyts, Patrick Dupont, Luc Mortelmans.
K.U.Leuven, dept. Nuclear Medicine, UZ Gasthuisberg, Herestraat 49, B3000 Leuven, Belgium

2nd IEEE workshop on *computer intensive methods in control and signal processing: can we beat the curse of dimensionality?* Prague, Czech Republic, August 28-30, 1996. K Warwick, M. Karny, eds. Birkhé4user, 1997: 237-248.

Abstract

In positron emission tomography (PET) transmission studies are acquired to compensate for photon attenuation. We have developed a simple gradient based maximum-likelihood (ML) algorithm for reconstructing the original distribution of attenuators from the transmission measurements. Our experiments show that attenuation compensation based on these reconstructions is superior to classical attenuation compensation based on the raw attenuation measurements.
The method has been extended for post-injection transmission studies, in which the transmission measurement is affected by photons originating from the injected tracer. This novel method was compared to ML-reconstruction after subtraction of the emission contribution, and to reconstruction/reprojection with filtered backprojection, indicating that the novel method suppresses noise better.
Finally, using a similar approach, a new ML-gradient algorithm was derived to compute both the attenuation and the activity distribution from the PET emission sinogram only. Simulations indicate that the emission sinograms indeed contain information on the attenuation distribution, which is recovered with the ML-approach. Application to clinical PET studies show promising results.

1. Introduction

In positron emission tomography (in 2D operational mode) parallel projections (line integrals along parallel straight) of a radioactive tracer distribution are acquired. Each pair of PET-detectors defines a single projection line, usually called line-of-response (LOR). The mathematical equivalent of this process is the Radon transform, written below in its digital form:

$$y_i = \sum_j c_{ij}\lambda_j, \qquad (1)$$

where y_i is the measured projection, λ_j the radioactivity at pixel j and c_{ij} the relative contribution of the activity at pixel j to the LOR at sinogram pixel i. If a sufficiently large set $\{y_i\}$ is known, the original distribution can be reconstructed.

In reality, there are two important deviations from the ideal Radon transform. First, because the radioactive dose must be limited, the measurements are strongly affected by Poisson noise. Second, a fraction of the photons is not detected due to attenuation (photon-electron interactions in the tissue of the patient). As a result, equation (1) must be modified into

$$y_i = \sum_j c_{ij}\lambda_j e^{-\sum_k c_{ik}\mu_k}, \qquad (2)$$

where μ_k is the linear attenuation coefficient in pixel k.

In the classical approach, the noise is suppressed by applying low-pass filtering. The attenuation problem is solved by measuring the total attenuation along a LOR with an external radioactive source. However, superior solutions to both problems can be obtained using iterative reconstruction. Maximum-likelihood (ML) expectation-maximization (EM) [1] has been shown to yield superior reconstruction of the emission images, by taking into account the Poisson nature of the measurements. Further noise suppression is achieved using maximum-a-posteriori algorithms [2] or by stopping the iterations before full convergence is achieved. ML-EM has been adapted to transmission tomography [3]. However, unlike in emission tomography, the complete variables introduced by the EM-algorithm do not cancel out in the final algorithm. In addition, a transcendental equation must be solved in every iteration. Ollinger [4] used Newton's method to solve that equation.

We followed an alternative approach, leaving the EM-algorithm and directly maximizing the likelihood function using a simple gradient algorithm. A disadvantage is that the Hessian matrix is not diagonal in this case, in contrast with the Hessian matrix of the M-step in the EM-algorithm [4]. An important advantage, however, is a reduction of the

complexity of the algorithm. This approach has been used in three applications:

1. Using ML-reconstruction of the transmission scan to improve the attenuation correction of the emission image.
2. ML-reconstruction of post-injection transmission studies, where an estimate of the undesired contribution of the administred emission tracer is available.
3. Simultaneous ML-reconstruction of both the attenuation and the activity distribution from the emission data, when no transmission scan is available.

2. Methods

2.1. Transmission

Applying Bayes rule and assuming that the a priori probability distributions p($\{y_i\}$) and p($\{\mu_j\}$) are homogeneous, the following relation holds:

$$p(\{\mu_j\}|\{y_i\}) \sim p(\{y_i\}|\{\mu_j\}) \tag{3}$$

Maximum likelihood reconstruction maximizes the expression at the right hand side in (3) (to simplify the algorithm, actually the logarithm of that expression is maximized). The logarithm of the Poisson distribution given the expected value λ equals:

$$\ln p(x|\lambda) = \ln \frac{\lambda^x e^{-\lambda}}{x!} = x \ln \lambda - \lambda - \ln(x!). \tag{4}$$

Applying this to the case of transmission tomography yields for the logarithm of the likelihood:

$$L = \sum_{i=1}^{I} \left(y_i \ln t_i - t_i - \ln(y_i!) \right), \tag{5}$$

$$t_i = b_i e^{-\sum_{j=1}^{J} c_{ij}\mu_j}. \tag{6}$$

where y_i is the transmission measurement, b_i is the blank scan value, I is the total number of sinogram pixels and J the total number of reconstruction pixels. The matrix of second derivatives of eq.(5),

$$\frac{\partial^2 L}{\partial \mu_k \partial \mu_l} = -\sum_{i=1}^{I} c_{ik} c_{il} t_i, \tag{7}$$

is negative definite, L is bounded from above and L goes to $-\infty$ when the norm of $\vec{\mu}$ goes to ∞, so L has a unique maximum. Therefore, the iterative algorithm of the form

$$\mu_j^{new} = \mu_j + \Delta\mu_j, \tag{8}$$

with $\Delta\mu_j$ the same sign as $\frac{\partial L}{\partial \mu_j}$ and $|\Delta\mu_j|$ sufficiently small, will converge.

We will estimate now the step $\Delta\mu_j$ in the neighborhood of the maximum $\vec{\mu}_0$. Expanding the first derivative up to first order, and assuming that $\Delta\vec{\mu}$ is such that $\vec{\mu} + \Delta\vec{\mu} = \vec{\mu}_0$, we obtain:

$$0 = \frac{\partial L}{\partial \mu_k}(\vec{\mu}+\Delta\vec{\mu}) = \frac{\partial L}{\partial \mu_k}(\vec{\mu}) + \sum_{l=1}^{J} \frac{\partial^2 L}{\partial \mu_k \partial \mu_l} \Delta\mu_l. \tag{9}$$

This implies that $\Delta\vec{\mu}$ should satisfy:

$$0 = \sum_{k=1}^{J} \left(\frac{\partial L}{\partial \mu_k}(\vec{\mu}) + \sum_{l=1}^{J} \frac{\partial^2 L}{\partial \mu_k \partial \mu_l} \Delta\mu_k \right). \tag{10}$$

Instead of solving eq.(9), which is much more complicated, we estimate $\Delta\vec{\mu}$ as:

$$\Delta\mu_k = -\frac{\frac{\partial L}{\partial \mu_k}(\vec{\mu})}{\sum_{l=1}^{J} \frac{\partial^2 L}{\partial \mu_k \partial \mu_l}(\vec{\mu})}. \tag{11}$$

This expression satisfies eq.(10) and has the same sign as $\frac{\partial L}{\partial \mu_k}$ since $\frac{\partial^2 L}{\partial \mu_k \partial \mu_l}(\vec{\mu}) < 0, \forall k,l$. Introducing a relaxation factor $\alpha > 0$, we monitor L such that the norm of $\Delta\vec{\mu}$ can be decreased if L happens to decrease. This leads to the following algorithm (which converges):

$$\mu_k^{new} = \mu_k + \frac{\alpha}{N} \left(1 - \frac{\sum_{i=1}^{I} c_{ik} y_i}{\sum_{i=1}^{I} c_{ik} b_i e^{-\sum_{j=1}^{J} c_{ij}\mu_j}} \right), \tag{12}$$

where we used the fact that $\sum_{j=1}^{J} c_{ij} = N$ for an image of $N \times N$ pixels. The main advantage of our algorithm is that we have a simple expression for $\Delta\vec{\mu}$ where the backprojection of the measurements needs only be calculated once, so every iteration requires one projection and one backprojection, as in the well known ML-EM algorithm for emission tomography [1].

In order to correct the emission study for attenuation, the reconstructed attenuation map must be reprojected to compute the attenuation correction factor A_i:

$$A_i = e^{\sum_k c_{ik}\mu_k}, \tag{13}$$

which must be multiplied with y_i to transform equation (2) into equation (1). The advantage of computing (13) instead of directly using the ratio of the blank b_i and the transmission measurement t_i (see equation 6) is that the reconstruction removes noise by discarding the inconsistencies in the projection data.

2.2. Post injection maximum-a-posteriori

In clinical practice, the scan duration can often be decreased considerably (with a concordant increase of patient comfort) by performing the transmission study after rather than before administration of

the tracer. Reconstruction of the attenuation map, then, requires correction for the undesired contribution of the emission tracer to the transmission study. The log-likelihood function now becomes:

$$L = \sum_{i=1}^{I} \left(y_i \ln(t_i + a_i) - t_i - a_i - \ln(y_i!) \right), \quad (14)$$

where we assume that an estimate of the expected tracer contribution a_i is available. Applying the same approach as above leads to

$$\Delta\mu_k = \alpha \left(-\frac{\partial L}{\partial \mu_k} \right) / \left(\sum_l \frac{\partial^2 L}{\partial \mu_k \partial \mu_l} \right) \quad (15)$$

$$= \frac{\alpha}{N} \frac{\sum_i c_{ik} \left(t_i - t_i \frac{y_i}{t_i + a_i} \right)}{\sum_i c_{ik} t_i \frac{t_i}{t_i + a_i}} \quad (16)$$

The denominator is a heuristic normalization factor, so it is acceptable to further approximate it. Assuming a_i is relatively small compared to t_i, and further assuming $t_i + a_i \simeq y_i$, the expression can be changed into

$$\Delta\mu_k = \frac{\alpha}{N} \frac{\sum_i c_{ik} \left(t_i - t_i \frac{y_i}{t_i + a_i} \right)}{\sum_i c_{ik} (y_i - a_i)}. \quad (17)$$

The advantage of this adaptation is that the denominator remains unchanged during the iterations, removing a costly backprojection from the computations.

In practice, only a Poisson realization of a_i is available (e.g. an emission measurement acquired immediately before the transmission study), whereas eq (17) assumes that a_i is free of noise. If $\bar{a}_i$ is the mean emission contribution, the variance on $y_i - (t_i + \bar{a}_i)$ would equal $t_i + \bar{a}_i$. Using the Poisson realization a_i, the variance increases to $t_i + 2\bar{a}_i \simeq t_i + 2a_i$, violating the assumption of Poisson noise that is the basis of the ML-algorithm. However, the Poisson characteristic can be restored approximately by setting

$$y_i' = y_i + a_i \quad (18)$$

$$a_i' = 2a_i \quad (19)$$

and applying the algorithm using y_i' as the measurement and a_i' as the known emission contribution.

Finally, because short scans are preferred, the noise on clinical data is mostly fairly large. To reduce the noise, an a-priori probability distribution of linear attenuation coefficients is included. Eq (3) becomes

$$p(\{\mu_j\}|\{y_i\}) = p(\{y_i\}|\{\mu_j\})\ p(\{\mu_j\}). \quad (20)$$

Consequently, the derivative of the logarithm of the prior must be added to the gradient of the likelihood in equation (17). The prior is defined as follows. A set of expected linear attenuation coefficients is defined, e.g. $\{\mu_{\text{air}}, \mu_{\text{lung}}, \mu_{\text{tissue}}\}$, together with a set of corresponding standard deviations. This defines a set of Gaussians. They are combined into a single function, by taking in each point the maximum of the Gaussian functions in that point. This produces an oscillating function with Gaussian-shaped maxima, and minima with discontinues first derivate (the points where the Gaussians intersect). The regions near the minima are modified to yield a continuous first derivative. The logarithm of this function consists of a piecewise parabolic function, the gradient is a piecewise linear function, which is easy to compute. This gradient is multiplied with a heuristic weighting factor and added to the numerator in (17).

2.3. Attenuation and activity from emission

In some clinical protocols, in particular on older 2D PET systems, the transmission scan is omitted in order to reduce the study duration because of patient comfort. This motivated us to try to reconstruct both the attenuation and the activity distribution from the emission study only. We have observed that the likelihood values reached by ML-EM reconstruction of emission studies is systematically lower when no attenuation correction is applied, suggesting that there is indeed information on the attenuation map present in the emission data.

The PET emission measurement can be predicted from the attenuation map μ_j and the activity distribution λ_j using

$$r_i = \sum_j c_{ij} \lambda_j\ e^{-\sum_k c_{ik} \mu_k} \quad (21)$$

This leads to the likelihood function

$$L = \sum_i (y_i \ln r_i - r_i - \ln y_i!) \quad (22)$$

The partial derivative with respect to λ_j is identical to that in the case of emission tomography with known attenuation. The partial derivate with respect to μ_j is identical to that in transmission tomography. Consequently, L can be optimized using iterated partial optimizations, applying one step of ML-EM followed by one step of the transmission algorithm (12). In the latter, the measurement is treated as a transmission study y_i, the unattenuated projection of the current reconstruction estimate is used as the blank scan b_i. In this case, the Hessian is not negative definite, so only convergence to a local maximum is guaranteed. In order to constrain the set of solutions, the likelihood function was extended with the a priori distribution for the attenuation coefficients, as outlined above. LORs which contain no activity provide no information about the attenuation: both the measurement y_i

and the computed blank b_i are zero. In this case, both y_i and b_i were set to an arbitrary positive constant. By setting $y_i = b_i = c > 0$, the algorithm is driven towards a solution with zero attenuation along LOR i. In clinical applications, this heuristic approach is often valid, because some activity accumulates in the skin.

3. Experiments

3.1. Transmission

A thorax phantom was measured with a 2D PET camera (CTI-Siemens, ECAT 931-8-12). The phantom consisted of a perspex elliptical cylinder (20 by 30 cm diameters), in which a cardiac (left ventricular) phantom (Data Spectrum Corp) was mounted. Also a polystyrene lung phantom was inserted, with the left lung touching the lateral wall of the heart phantom. The wall of the cardiac phantom was filled with a homogeneous activity (35 MBq ^{18}F in 115 ml, $t_{1/2}$ = 109.7 min), the cavity of the cardiac phantom and the elliptical cylinder were filled with cold water. A long emission scan (5 h) was acquired in order to obtain low noise attenuated emission sinograms. After decay of the activity (50 hours), one long and two short transmission studies were performed (4 hours, 1 min and 8 min), using 8 ring sources with approximately 58 MBq per ring. The phantom was removed from the camera and a long blank scan was acquired.
Three different attenuation methods were applied: A) the classical approach: the ratio of the blank and tranmission scan (both smoothed 0, 1, 2, 3 and 4 times with the Gaussian filter supplied by the manufacturer). B) reconstruction of the attenuation map by filtered backprojection, followed by reprojection. This reduces the noise in the attenuation correction factors, although the noise reduction in the final attenuation corrected emission image is limited [5, 6]. Again the same series of Gaussian filters was applied. C) attenuation correction factors derived from ML-reconstruction of the transmission scan. Noise suppression was obtained by stopping at iteration number 10, 30, 100, 300 and 1000. This resulted in 15 sets of attenuation correction factors per transmission study, which were used in the reconstruction of the low noise emission study with filtered backprojection. As a reference, the emission study was also reconstructed using attenuation correction factors derived from the long transmission study, using the classical method without smoothing. The emission reconstructions were compared by computing the square root of the mean squared difference with the reference image.

3.2. Post injection maximum-a-posteriori

A simple single slice cardiac model was simulated, with a linear attenuation coefficient of 0.1 cm^{-1} in tissue and 0.33 cm^{-1} in the lung. The activity in the heart was 6 times higher than in the lungs and in the background. The slice contained 100 x 100 pixels, with a pixel size of 3.33 mm. The maximum count in the emission sinogram was 32, and in the transmission sinogram 100. Both were first multiplied with a different scale factor, simulating different relative and absolute contributions, the scaled sinograms were summed and Poisson noise was added to produce the post-injection transmission sinogram. In addition, independent Poisson noise was added on the emission sinogram to produce a noisy estimate of the emission contribution. Consequently, higher blank scales result in lower relative noise, higher emission scales in a higher undesired contribution.

Each set of images was used to compute attenuation correction factors in four different ways:

mlpost Post-injection ML-algorithm, combined with Gaussian priors, as described above.

ml Estimated emission was subtracted from the transmission sinogram. The result was reconstructed using the ML-transmission algorithm, combined with Gaussian priors.

reproj Estimated emission was subtracted from the transmission sinogram. The result was reconstructed using filtered backprojection and reprojected.

fbp Estimated emission was subtracted from the transmission sinogram. The ratio of the blank and this corrected sinogram was used for attenuation correction.

For each pair of scale factors, a normalized squared difference between the resulting image and the reference was computed, both for the reconstructed attenuation map and the reconstructed emission image. For the ML-algorithms, a large range of weighting factors for the prior distribution was used (over four orders of magnitudes, in steps of 20%). For the two other techniques, 11 different smoothing filters were applied. For each algorithm and each pairs of scales, the best results were selected for final comparison.

3.3. Attenuation and activity from emission

Two different artificial objects were simulated to evaluate the performance of the new algorithm in ideal conditions. The first consisted of two overlapping ellipses, the other was a cross-shaped object. In both cases, the object contained significant concavities, which are most challenging for our algorithm. In both cases, the attenuation in the object was uniform, and zero outside. The entire attenuating object contained non-zero and non-uniform

activity. A 1000 iterations were executed. A prior with two attenuation coefficients (object and air) was used.

The same algorithm was then applied to a clinical PET-study (an 80 cm, 120 slices acquisition of the lower limbs), using the known attenuation coefficients of tissue and air for the prior.

4. Results

4.1. Transmission

For the short (1 min) transmission study, the ML-based attenuation correction using 10 and 30 iterations produced equivalent emission reconstructions, which were clearly superior (quantified deviation 50% lower) to those of the other two methods. For the latter, best results were obtained with a single smooth with the Gaussian filter. Reconstruction with attenuation correction based on reprojected transmission scans were superior to those obtained with the classical approach (quantified deviation 20 % lower). For the 8 min scans, the difference between the methods was very small. Best results were obtained using 30 iterations for ML, and a single Gaussian smooth for the other two methods.

4.2. Post injection maximum-a-posteriori

The quantified difference between the resulting emission and transmission reconstruction and the respective reference images is tabulated in table 1.

4.3. Attenuation and activity from emission

Figure 1 shows the result of 1000 iterations of the new algorithm, compared to the reference image and to 20 iterations of ML-EM without attenuation correction. The new algorithm converged slowly: there was a small but noticeable difference between iteration 500 and iteration 1000.

On the patient study, convergence was much faster because the contours of the attenuating objects are nearly convex. The resulting attenuation map shows a correct anatomical shape, although in some slices local reconstruction errors were observed.

5. Discussion

In contrast to the findings in [5, 6], we observed that reprojection of filter-backprojected transmission images yielded superior attenuation corrected images, as compared to the classical approach. This may be explained by the fact that in our experiment, both the attenuation and the emission distribution were inhomogeneous, whereas the experiments and derivations in [5, 6] were done for homogeneous and radially symmetrical cases.

The attenuation correction based on ML-reconstruction produced significantly superior results when the noise contents of the sinogram was large. For sinograms with better signal to noise ratio, the difference in performance is negligible. This finding suggests that the use of the exact Poisson model enables ML to discard a larger fraction of the noise in the sinogram, as compared to the classical methods.

Similarly, the more exact post-injection transmission algorithm (mlpost in table 1) performed better than ML after subtraction (ml), and far better than the other two methods (reproj, fbp), when the contribution of the emission was significant. However, the difference between the two ML-methods (mlpost, ml) became smaller when the emission contribution was lower, or when the relative noise amplitude decreased. The only aberrant finding is the poor performance of post-injection ML as compared to the other methods for the second column in table 1, which we currently cannot explain. Note, however, that the inclusion of the prior distribution changes the likelihood function, and as a result, it is no longer guaranteed that there is a unique maximum. Possibly, the ML post-injection algorithm was trapped in a local maximum, which happened to be avoided by the different convergence path of the ML-transmission path. Note, however, that additional constraining (stopping the iterations or using MAP) is needed to prevent the ML-algorithm to include too much noise from the projections into the reconstruction.

Censor et al [7] reported limited success with the computation of attenuation on a pixel by pixel basis from emission sinograms using an iterative procedure named "cyclic subgradient projections". More recently, Natterer [8] has investigated the possibility to derive attenuation information using a much more constraint model, where the attenuation map was defined by a parameterized contour and a constant attenuation coefficient.

Here, we have again shown that, at least in an ideal case, a large amount of information on the attenuation distribution can be extracted from the emission data. The advantage of the ML-approach is not only that Poisson noise is correctly dealt with, but also that the inclusion of a-priori knowledge is relatively easy and that much experience with these methods is available.

The attenuation map obtained from the clinical emission study corresponded well to the gross anatomy of the attenuator, but in some slices, regional reconstruction errors were observed. This attenuation map should be a good input for a segmentation algorithm. However, we believe that with inclusion of more a-priori knowledge the performance

scale	blank	1.00	1.00	1.00	1.00	4.00	4.00	4.00	16.00	16.00	16.00
	emission	0.00	1.00	4.00	16.00	1.00	4.00	16.00	1.00	4.00	16.00
emission	mlpost	0.96	1.62	1.74	2.01	0.84	0.95	1.33	0.67	0.77	0.84
	ml	0.95	1.54	1.93	2.13	0.82	1.03	1.52	0.67	0.74	0.83
	reproj	1.20	1.55	2.21	3.76	1.09	1.37	1.68	0.88	0.97	1.12
	fbp	1.19	1.68	2.57	4.26	1.09	1.36	1.95	0.86	0.95	1.11
transmission	mlpost	0.44	0.66	0.73	0.92	0.34	0.39	0.50	0.26	0.29	0.33
	ml	0.43	0.63	0.85	1.09	0.36	0.48	0.64	0.25	0.29	0.35

Table 1: Top: The scales used to modify the relative contributions of transmission and emission counts. Center: the error on the emission reconstruction for the four algorithms. Bottom: the error on the transmission reconstruction (no reconstruction is made in classical attenuation correction).

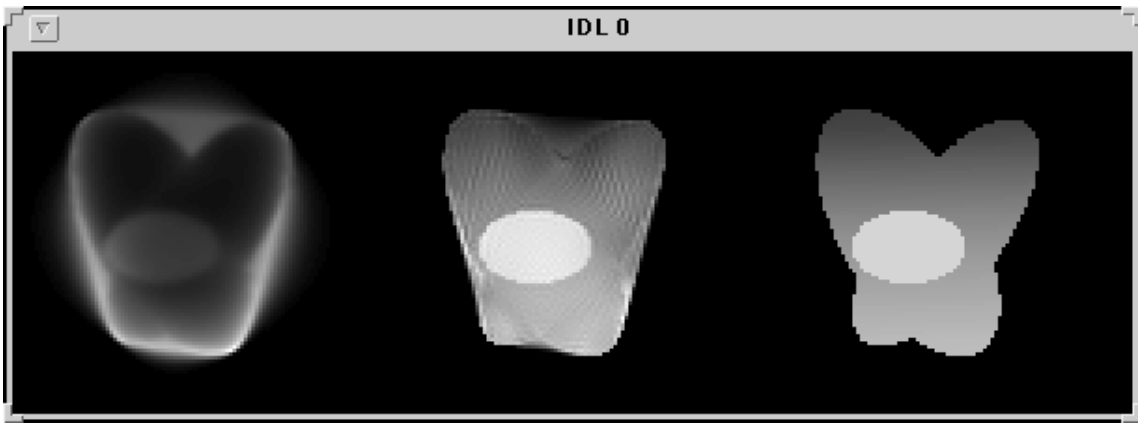

Figure 1: Left: 20 ML-EM iterations without attenuation correction. Center: 1000 iterations of the combined emission-transmission ML-algorithm. Right: the reference image.

of the algorithm can be further enhanced.

6. Conclusion

The experiments indicate that correct modeling of the noise in the sinogram does improve the quality of the resulting attenuation correction or reconstruction.
Direct optimisation of the likelihood function using a simple gradient approach has the advantage of being flexible (adaptation to the post-injection application is trivial) and leading to simple projection/backprojection algorithms. A disadvantage is that a relaxation factor must be introduced in order to guarantee convergence.

References

[1] LS Shepp, Y Vardi. "Maximum likelihood reconstruction for emission tomography". *IEEE Trans Med Imaging*, vol MI-1, pp 113-122, 1982.

[2] EU Mumcuoglu, R Leahy, SR Cherry, Z Zhou. "Fast gradient-based methods for Bayesian reconstruction of transmission and emission PET images." *IEEE Trans Med Imaging*, vol 13, pp 687-701, 1994.

[3] K Lange, R Carson. "EM reconstruction algorithms for emission and transmission tomography." *J Comput Assist Tomogr*, vol 8, pp 306-316, 1984.

[4] JM Ollinger. "Maximum-likelihood reconstruction of transmission images in emission computed tomography via the EM algorithm." *IEEE Trans Med Imaging*, vol 13, pp 89-101, 1994.

[5] JM Ollinger. "Reconstruction-reprojection processing of transmission scans and the variance of PET images." *IEEE Trans Nucl Sci*, vol 39, pp 1122-1125, 1992.

[6] BTA McKee, LG Hiltz, PJ Harvey. "Signal-to-noise ratios for attenuation correction in PET imaging." *IEEE Trans Med Imaging*, vol 13, pp 711-715, 1994.

[7] Y Censor, DE Gustafson, A Lent, H Tuy. "A new approach to the emission computerized tomography problem: simultaneous calculation of attenuation and activity coefficients."

IEEE Trans Nucl Sci, vol NS-26, pp 2775-2779, 1979.

[8] F Natterer. "Determination of tissue attenuation in emission tomography of optically dense media." *Inverse Problems*, vol 9, pp 731-736, 1993.